Molecular Ball Joints: Mechanochemical Perturbation of Bullvalene Hardy-Cope Rearrangements in Polymer Networks

Peiguan B. Sun[1], Meredith N. Pomfret[1], Matthew J. Elardo[1], Progyateg Chakma[1], Sheila Keating[2], Chuqiao Chen[2], Yunze Wu[1], Rowina C. Bell[1], Stuart J. Rowan[2], Matthew R. Golder[1]*

[1] Department of Chemistry and Molecular Engineering & Science Institute, University of Washington, Seattle, WA 98115
[2] Pritzker School of Molecular Engineering, University of Chicago, Chicago, IL 60637

Abstract:

The solution-state fluxional behavior of bullvalene, first investigated over 60 years ago, has fascinated physical organic and supramolecular chemists alike. Little effort, however, has been put into investigating bullvalene applications in the bulk, partially due to difficulties in characterizing such dynamic systems. To address this fundamental knowledge gap, herein we probe whether bullvalene Hardy-Cope rearrangements can be mechanically perturbed in bulk polymer networks. We first demonstrate the impact of bullvalene fluxionality in bulk thermoset elastomers using modulated differential scanning calorimetry; enhanced enthalpic relaxation events are observed in the non-reversing heat flow for bullvalene-containing materials relative to "static" control networks. Then, we use dynamic mechanical analysis to demonstrate that the activation barrier to glass transition is significantly elevated for bullvalene-containing materials (ca. 90 kcal/mol) relative to "static" control networks (ca. 50 kcal/mol). Furthermore, bullvalene rearrangements can be "mechanically activated" at low temperature in the glassy region; such behavior facilitates energy dissipation (at least ca. 3-fold increase in hysteresis energy) and polymer chain alignment to stiffen the material (at least ca. 2-fold increase in Young's modulus) under load. Collectively, this work showcases bullvalene as a reversible chemical mechanophore in the modulation of viscoelastic behaviors.

Introduction:

Ever since the first syntheses by Doering, Roth and Schröder in the 1960s, bullvalene has fascinated chemists due to its unique molecular architecture.[1,2] Three alkenes emanating from a central carbon atom, organized symmetrically in a boat conformation, and connected by a strained cyclopropane ring sets up ideal conditions for rapid Hardy-Cope rearrangements.[3] Unsubstituted bullvalene has more than 1.2 million (10/3!) degenerate isomers rapidly interconverting (E_a = ca. 11 kcal/mol) at room temperature (**Figure 1A**).[4,5]

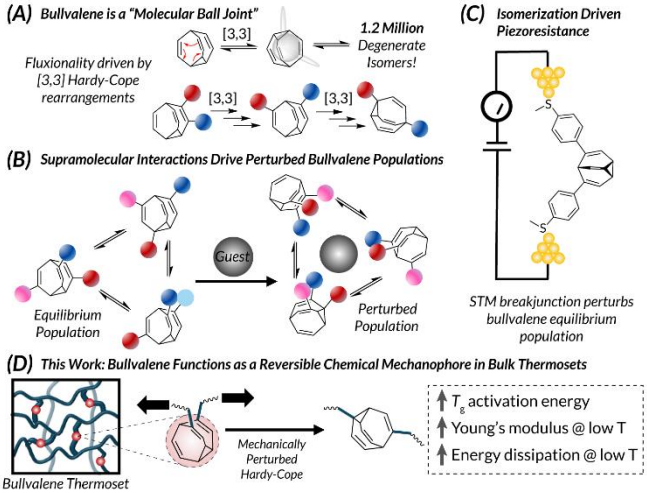

Figure 1: (**A**) Illustration of rapid bullvalene Hardy-Cope rearrangements; (**B**) Bullvalene adjusts equilibrium population upon guest-host interactions; (**C**) Bullvalene employed as single molecule circuit junction; (**D**) Proposed mechanochemical perturbation of bullvalene equilibrium population in bulk polymer networks

Supramolecular interactions can perturb the interconversion of fluxional isomers for applications in molecular recognition (**Figure 1B**).[6-9] Such substituted bullvalenes, when unperturbed, exist in an equilibrium distribution of valence isomers. Upon addition of analytes, bullvalene engages in guest-host interactions, shifting to a new equilibrium population. Accessing such multi-substituted bullvalenes, however, is difficult due to lengthy synthetic sequences.[10,11] Recent progress in concisely accessing substituted bullvalenes reported by Fallon reignited interest for bullvalene applications.[12,13] Most applications of bullvalene explored so far are solution-state, however. Interestingly, examples of bullvalene rearrangements in the solid-state also exist.[14,15] Specifically, dynamic behaviors were observed in unsubstituted bullvalene single crystals with an activation barrier for Hardy-Cope rearrangements resembling those in isotropic and liquid crystalline solutions. More recently, Darwish and Fallon demonstrate that when bullvalene is introduced to a scanning tunneling microscopy breakjunction (STMBJ), its rapid isomerism facilitates dynamic piezoresistance (**Figure 1C**).[16] Our previous work incorporated bullvalene into π-rich thermoplastics showing that stochastic bullvalene isomers could effectively modulate the rigidity of such polymers but left many unanswered questions about resultant thermomechanical behaviors.[17]

Recent advances in polymer mechanochemistry have led to the development of force responsive materials.[18,19] Incorporating force-responsive small molecules (e.g., mechanophores) into polymer networks introduces novel properties such as strain toughening,[20] cargo release,[21,22,23] stress visualization,[24,25,26] and tear resistance.[27] These systems can generally be separated into two categories – physical and chemical. Physical systems take advantage of structural adaptations to external forces (i.e., bond rotations, non-covalent interactions); specific examples include soft materials containing "expandable",[28,29,30] mechanically-interlocked,[31-35] hydrogen-bonded,[36-39] and/or metal-ligated elements.[40-46] Adaptations in these systems are generally reversible with low activation barriers. On the other hand, systems bearing chemical mechanophores use high energy barrier chemical transformations to adapt to applied mechanical force (e.g., cyclo-reversion)[20-24, 27]; such processes are irreversible, however.

Since bullvalene's valence isomer distribution can adapt to exogenous stimuli in solution and in the bulk (**Figure 1**),[6-8,14-16] we imagined that upon applied mechanical force within a bulk material, the equilibrium population of bullvalene could adapt to the applied force vector. We envisioned that studying the thermomechanical properties of these materials would be an ideal way to understand molecular-level sigmatropic rearrangements within polymer networks. If reversible Hardy-Cope rearrangements can be perturbed through mechanical force, we might expect unique thermoset properties by bridging the gap between physically and chemically responsive systems (**Figure 1D**). Herein, we incorporate bullvalene into elastomeric polymer networks to study their thermal behavior and temperature-dependent viscoelastic properties alongside control networks containing "static" crosslinkers. Using a combination of differential scanning calorimetry (DSC) and dynamic mechanical analysis (DMA), we demonstrate that bullvalene rearrangements not only increase the glass transition activation barrier, but also lead to distinct stiffening and energy dissipation behaviors below the glass transition temperature (i.e., glassy region). These collective thermal and mechanical properties unique to bullvalene thermoset elastomers provide credence for the consequences of molecular fluxionality on bulk materials properties.

Results and Discussion:

The requisite crosslinked elastomers for thermal and mechanical testing were synthesized from *n*-butyl acrylate and an appropriate diacrylate crosslinker under thermal free radical conditions (V-70, 60 °C) that we have confirmed bullvalene tolerates (**Figure S1**). We selected a crosslinker loading of 7 mol% to minimize the impact of chain entanglement and maximize the impact of crosslinker structure and ease of material preparation. The crosslinker for target bullvalene network (**Bull-Net-7**), bullvalene diacrylate (**Bull-DA**), is derived from dimethanol bullvalene **5**, the product of Co-catalyzed formal [6+2] cycloaddition of silyl-protected 2-butyne-1,4-diol **2** and cyclooctatetraene (COT) after deprotection.[5,12,47] Photochemical di-π-methane rearrangement[48,49,50] to **4** and subsequent esterification with acrylic acid

affords **Bull-DA** over 5 steps (**Scheme 1A**). In the selection of control "static" crosslinkers, we first chose adamantane diacrylate **(Ad-DA).** Bullvalene and adamantane are both C_{10} hydrocarbon cages with similar molar masses. Conveniently, substituents on adamantane are also situated in a non-planar fashion, akin to bullvalene's geometry. As **Bull-DA** and **Ad-DA** should therefore have similar steric profiles, we can probe the effect of crosslinker topology and fluxionality on bulk materials properties through synthesis of **Ad-Net-7**. Apart from the impact of crosslinker bulkiness, we also controlled for bullvalene substituent sigma-bond rotations by utilizing commercially available 1,6-hexanediol diacrylate (**Hex-DA**) as a second control crosslinker towards **Hex-Net-7** (**Scheme 1B**).

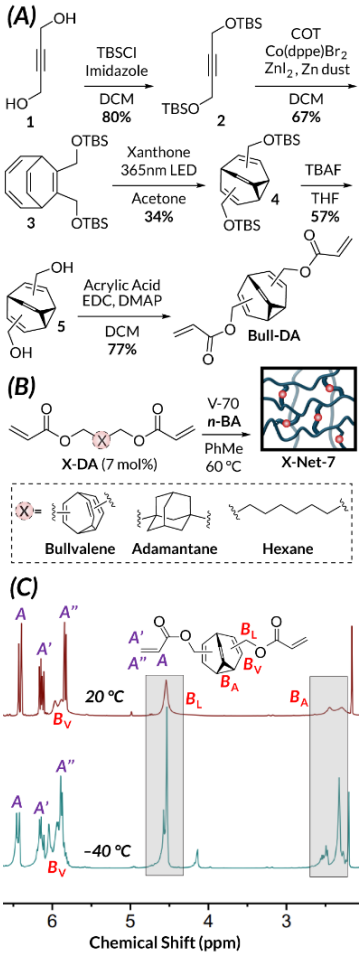

Scheme 1: (**A**) Synthesis of bullvalene diacrylate crosslinker (**Bull-DA**); (**B**) Preparation of crosslinked *n*-butyl acrylate polymer networks (**Bull-Net-7**, **Ad-Net-7**, **Hex-Net-7**); (**C**) ^{1}H NMR spectra (500 MHz, $CDCl_3$) of **Bull-DA** at 25 °C and –40 °C

To glean insight to potential temperature-dependent phenomena in **Bull-Net-7**, solution-state variable temperature NMR (VT-NMR) experiments (**Scheme 1C**) were conducted on **Bull-DA** that reveals slow chemical exchange at room temperature consistent with E_a = ca. 11 kcal/mol; broad bullvalene vinyl proton (B_V), alkyl proton (B_A) and methylene linker proton (B_L) resonances around 5.9 ppm, 2.3 ppm, and 4.5 ppm, respectively support this claim. When **Bull-DA** is cooled to –40 °C, B_V, B_A and B_L resonances sharpen as the rate of chemical exchange via thermal Hardy-Cope rearrangements decreases further and approach a static structure. Meanwhile, proton resonances not directly connected to the bullvalene cage (*A*, *A'*, *A''*) actually broaden as bond rotation (E_a < 3 kcal/mol) slows on the NMR timescale. The differing dynamics between the chemical (i.e., bullvalene Hardy-Cope rearrangements) and physical (i.e., bond rotations) allows us to tame bullvalene fluxionality at lower temperatures, rendering bullvalene nearly static and

confining it to a smaller quantity of valence isomers. In order to probe mechanochemical activation of Hardy-Cope rearrangements in bulk materials, we reasoned that experiments needed to be conducted at lower temperatures where thermal bullvalene fluxionality is suppressed.

The physical properties of the resulting networks (ca. 80% monomer conversion) **Bull-Net-7**, **Ad-Net-7**, and **Hex-Net-7** were characterized using a variety of analytical techniques. Thermal gravimetric analysis (TGA, **Figure S2**) confirms that all materials have similar decomposition temperatures (T_d = 364 – 377 °C) and helium pycnometry demonstrates that all materials have the same densities (ρ = 1.06 – 1.09 g/cm^3, **Table S1**) at 25 °C. Tensile plateau moduli (E'_0) measured using DMA frequency sweep experiments at 20 °C confirm that all materials have E'_0 (0.261, 0.269, 0.405 MPa for **Bull-Net-7**, **Ad-Net-7**, **Hex-Net-7**, respectively) on the same order of magnitude, and thus have similar entanglement molecular weights (**Figure 4**). The glass transition temperatures of the materials were characterized through modulated differential scanning calorimetry (MDSC). Analysis of the total heat flow shows that **Bull-Net-7** and **Ad-Net-7** have similar $T_{g,DSC}$ (–29 °C and –33 °C, respectively) (**Figure 2A**). **Hex-Net-7** has a slightly lower $T_{g,DSC}$ (–42 °C), likely due to reduced crosslinker rigidity.[51] We also performed swelling experiments in several organic solvents (methylene chloride, acetone, ethyl acetate, dimethylformamide) to compare crosslinking densities across all materials (**Figure S3)**. While **Bull-Net-7** consistently has the highest equilibrium swelling ratios, they are generally within 10 – 15% that of **Ad-Net-7**. We attribute the inconsistencies in swelling ratios to differences in crosslinker sterics (in the case of **Bull-Net-7** and **Ad-Net-7**) and crosslinker fluxionality (in the case of **Bull-Net-7**) that may facilitate increased swelling. Nevertheless, due to the similarities in monomer conversion, T_d, ρ, $T_{g,DSC}$, and E'_0 across **Bull-Net-7**, **Ad-Net-7**, and **Hex-Net-7**, we assume that network structures are comparable for the purposes of thermomechanical analyses.

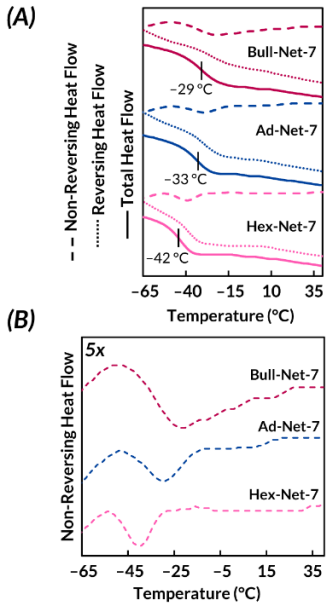

Figure 2: (**A**) MDSC curves of **X-Net-7** materials; (**B**) Expanded (5x) non-reversing heat flow curves from MDSC

With these comparable thermoset elastomers in hand, we further explored their thermal behavior using MDSC. Interestingly, we see a different enthalpic relaxation profile in the kinetic process driven, non-reversing heat flow in **Bull-Net-7** (**Figure 2B**). As **Ad-Net-7** and **Hex-Net-7** relax to equilibrium following their respective glass transition events, **Bull-Net-7** has a seemingly prolonged relaxation. In addition, both **Ad-Net-7** and **Hex-Net-7** show clear glass transitions in the reversing heat flow, but **Bull-Net-7** total heat flow is dominated by enthalpic relaxation; only a small glass transition is seen in the reversing heat flow.

Accounting for the low bullvalene loading in **Bull-Net-7**, this difference in relaxation profile could be caused by the drastic increase in molecular mobility at the onset of $T_{g,DSC}$, thereby bringing additional degrees of freedom for bullvalene rearrangements and broadening the enthalpic relaxation event.

With an enhanced understanding of **Bull-Net-7** thermal behavior, we next turned to thermomechanical analysis. First, DMA temperature sweep experiments were performed under tension (1 Hz); thermomechanical $T_{g,DMA}$ of **Bull-Net-7**, **Ad-Net-7**, and **Hex-Net-7** were measured to be 4.6 °C, –9.1 °C and –18 °C, respectively (**Figure 3A**), at the apex of each Tan (δ) peak. **Bull-Net-7** has the broadest Tan (δ) peak which suggests a more complex damping mechanism relative to **Ad-Net-7** and **Hex-Net-7**. It should be noted that while the span of $T_{g,DMA}$ values is larger than for $T_{g,DSC}$, the *onset* of $T_{g,DMA}$ is quite similar across all materials. To quantify differences in these thermomechanical glass transition processes, the respective activation energies were calculated through multi-frequency temperature sweep experiments and fitting to the Arrhenius equation (**Figure 3B**, **Figures S4-S6**).[52] Here, E_a for **Bull-Net-7** $T_{g,DMA}$ (89.7 kcal/mol) is ca. 75% higher than for **Ad-Net-7** (48.2 kcal/mol) and **Hex-Net-7** (51.0 kcal/mol). This elevated E_a for **Bull-Net-7** could be caused by an increase in fluxional rearrangements as the material approaches the glass transition temperature. Below $T_{g,DMA}$, long range segmental motion is restricted and bullvalene has access to only a few immediate isomers that do not bring structural changes to the polymer network. As the temperature continues to rise while approaching $T_{g,DMA}$, molecular mobility dramatically increases. Consequently, there are more degrees of freedom for bullvalene to access additional isomers while adapting to the external force vector through a series of Hardy-Cope rearrangements. In doing so, energy is dissipated within the bullvalene cage (i.e., additional energy is required for sigmatropic rearrangements) and the observed E_a for **Bull-Net-7** is elevated relative to those of the control networks.

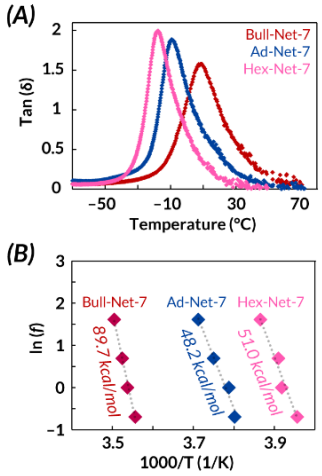

Figure 3: (**A**) Temperature sweep experiments (1 Hz) of **X-Net-7** materials; (**B**) Arrhenius plots of $T_{g,DMA}$ of **X-Net-7** materials

All materials were then subjected to frequency sweep experiments using DMA. In these experiments, we studied thermomechanical behavior at room temperature (20 °C, **Figures 4A and 4C**) where bullvalene remains fluxional, and below all materials' $T_{g,DMA}$ (–40 °C, **Figures 4B** and **4D**) where bullvalene is virtually static (**Scheme 1C**). At 20 °C, only minor mechanical differences are observed across the three materials. For example, the storage modulus (E') of **Hex-Net-7** is not sensitive to frequency, while **Bull-Net-7** and **Ad-Net-7** show a slow increase in E' above 10 Hz. Across all frequencies, **Bull-Net-7** has the highest Tan (δ) values and therefore the highest damping capacity. Despite these minor differences, the moduli of all materials are similar at 20 °C.

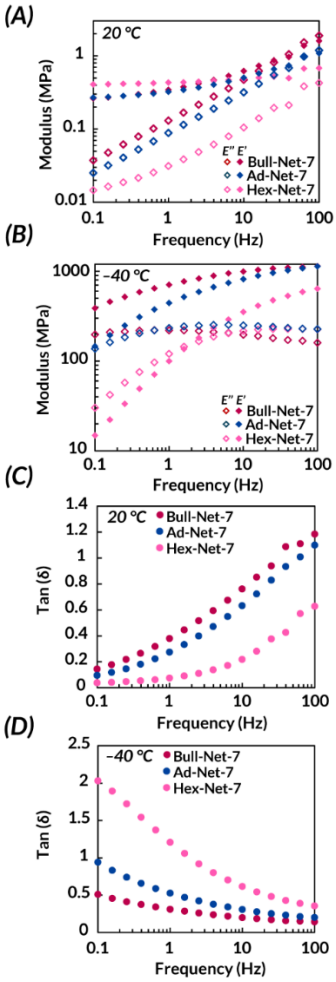

Figure 4: *E*' and *E*'' from frequency sweep experiments of **X-Net-7** materials at (**A**) 20 °C, (**B**) –40 °C; Tan (δ) curves at (**C**) 20 °C, (**D**) –40 °C

Interestingly, thermomechanical behaviors become more disparate at –40 °C (**Figure 4C and 4D**). The transition between the glassy and rubbery states usually entails large changes in *E*'. Starting with nearly identical *E*' at 20 °C, **Bull-Net-7** and **Ad-Net-7** *E*' at –40 °C increases to 388 MPa and 137 MPa, respectively (0.1 Hz). Across all frequencies, **Bull-Net-7** also has the lowest Tan (δ), signifying an increase in stored elastic energy relative to heat dissipation. The contrast in **Bull-Net-7** Tan (δ) between 20 °C and –40 °C can be explained by the fact that bullvalene is dynamic at room temperature and can rapidly sample an ensemble of valence isomers. Above $T_{g,DMA}$ at 20 °C, molecular motion is rapid; polymer chains can slide past one another and the bulky crosslinker can rotate. The rapid bullvalene fluxionality alongside freedom in molecular and chain mobility renders **Bull-Net-7** similar to **Ad-Net-7**. However at –40 °C, such macromolecular motion is limited and bullvalenes are largely static. As energy is applied through oscillatory tension in frequency sweep experiments, bullvalene rearranges to applied mechanical force, storing more energy elastically at lower frequency. As the frequency increases, the rate of mechanochemical Hardy-Cope rearrangements become convoluted with the rapid deformation of the material, thus making it difficult to distinguish **Bull-Net-7** from **Ad-Net-7** at higher frequency (e.g., 100 Hz).

Further examination of **Bull-Net-7** energy dissipation behavior was carried out using DMA via cyclic loading experiments. At 20 °C, **Bull-Net-7**, as well as control networks **Ad-Net-7** and **Hex-Net-7**, display minimal hysteresis (**Figure 5A, Figure S7 - S9**) and have similar Young's moduli (E = 0.0022 – 0.0038 MPa, **Table S2**). When the same cyclic loading experiments were carried out at –40 °C (**Figure 5B**, **Figures**

S10 – S15), all materials display strain-stress curves known for glassy polymer with little immediate recovery upon unloading.[53,54] While **Hex-Net-7** is extremely soft, **Ad-Net-7** has noticeable energy dissipation characteristics (E_H = 2110 J/m^2); **Bull-Net-7** has nearly three-times the hysteresis energy of **Ad-Net-7** (E_H = 6240 J/m^2, **Figure 5C**) with enhanced stiffening (E = 8.5 MPa, **Table S3**).

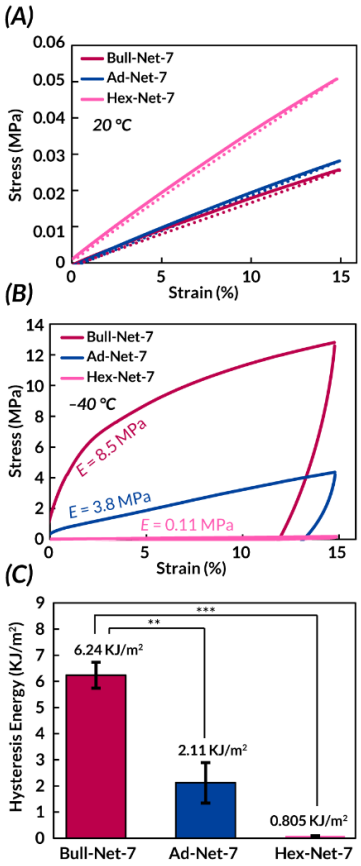

Figure 5: Cyclic loading of **X-Net-7** at (**A**) 20 °C, (**B**) –40 °C; (**C**) Hysteresis energies of **X-Net-7** materials (two-tailed t-test, n = 3; **: $p < 0.01$, ***: $p < 0.001$) with respective Young's moduli inset.

It should be noted that the mechanism of deformation in materials below glass transition is different from conventional viscoelastic behavior above T_g. Instead of long-range disentanglement through chain sliding, bond cleavage and local molecular motion generally dominate.[51,53,54] Repeated cyclic loading of all **X-Net-7** materials at –40 °C does not show loss in mechanical performance, thus confirming that minimal covalent bond cleavage occurs at low temperature in **X-Net-7** materials.

To confirm that this behavior (**Figure 5**) is not due to variations in material density below $T_{g,DMA}$, we performed thermal expansion experiments at –40 °C (**Figure S16**). As no significant differences were observed between **Bull-Net-7** and **Ad-Net-7**, corroboration with pycnometry data (**Table S1**) implies comparable low temperature densities. Based on these collective data, crosslinker sterics may be more impactful in regulating low temperature viscoelastic properties as significant hysteresis is observed for both **Bull-Net-7** and **Ad-Net-7**. In turn, the observed differences in hysteresis energies may be attributed to differences in the relative stiffness and yield stress of these material. For example, **Bull-Net-7** has a much higher Young's modulus (8.5 MPa) relative to controls **Ad-Net-7** and **Hex-Net-7** (3.8 MPa and 0.11 MPa respectively). We hypothesize that upon cooling, bulky crosslinkers take up more space, aligning the soft polymer chains tighter than allowed in **Hex-Net-7**. This steric driven bundling of polymer chains and subsequent freezing at temperatures below $T_{g,DMA}$ ultimately stiffens **Ad-Net-7** and **Bull-Net-7** (**Figure 6A**).

Importantly, unlike sterically demanding adamantane, similarly sized bullvalene rearranges upon applied mechanical force, (i.e., "molecular ball joint") to further realign the already packed polymer strands together and make the material stiffer (**Figure 6B**). Additionally, without free segmental motion, the initial input mechanical energy can be first "absorbed" in **Bull-Net-7** by bullvalene rearrangements and the subsequent realignment of polymer chains. The result is that **Bull-Net-7** has a much higher yield stress (ca. 6 MPa at ca. 2% strain) compared to **Ad-Net-7** (yield stress < 1 MPa at < 1% strain) in the shear yielding process.[53,54] In other words, at low temperatures **Bull-Net-7** has increased stiffness and yield stress relative to control networks; these properties contribute to a sigmatropic rearrangement driven, sterically enhanced high hysteresis energy for **Bull-Net-7**. These phenomena are not limited to **X-Net-7**, analogous thermosets with 2 mol% crosslinker loading (**Bull-Net-2** and **Ad-Net-2**) also have similar tensile properties (**Figure S17 and S18**). Furthermore, these processes were all demonstrated to be fully reversible; when **X-Net-7** materials are allowed to warm to room temperature between successive loading at –40 °C minimal changes in the resulting stress-strain curves are observed (**Figure S19 – S21**).

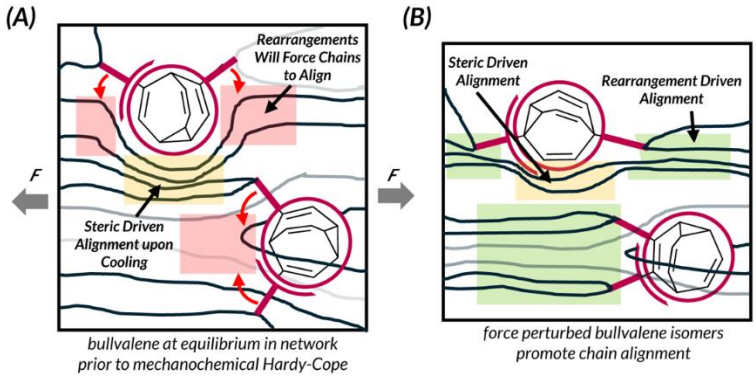

Figure 6: (**A**) Bullvalene adapts to applied force (**B**) through chain alignment governed by mechanically-guided Hardy-Cope rearrangements

Conclusion:

In summary, we report the utility of low barrier Hardy-Cope rearrangements under strain in polymer networks by incorporating fluxional bullvalenes into *n*-butyl acrylate-based thermoset elastomers. MDSC demonstrates that the glass transition in **Bull-Net-7** materials involve more complex relaxation processes compared to "static" crosslinked thermosets. DMA temperature sweep experiments quantitatively demonstrate that bullvalene can dissipate energy more effectively than "static" controls, thereby increasing the activation energy for the glass transition. While thermomechanical testing supports similar behavior between bullvalene (**Bull-Net-7**) and bulky adamantane (**Ad-Net-7**) crosslinked materials at room temperature, as the rate of bullvalene Hardy-Cope rearrangements decrease at lower temperature to afford a nearly static structure, frequency sweep experiments suggest rearrangements can be activated mechanochemically. Such a paradigm facilitates increased elastic energy storage in **Bull-Net-7**. Finally, cyclic loading experiments at –40 °C demonstrate that **Bull-Net-7** is much stiffer with high hysteresis energy. Soft **Hex-Net-7** with minimal observed hysteresis supports the hypothesis that low barrier sigma-bond rotations are not responsible for the observed **Bull-Net-7** properties. Comparisons against **Ad-Net-7** suggests that the topology of the bulky crosslinker contributes to unique low temperature **Bull-Net-7** behavior but is not the only factor. Rather, bullvalene's ability to rearrange upon applied mechanical force further facilities chain alignment and stiffens the material upon loading. Overall, having a simple unimolecular "ball joint" moiety that can dissipate energy through reversible sigmatropic rearrangements shows great potential for enhancing the durability of existing thermosets and opens new opportunities for impact and vibration resistant materials.

Author Contributions:
P.B.S. and M.R.G. conceived of the idea. P.B.S., M.N.P., M.J.E., and Y.W. synthesized small molecules. P.B.S. and P.C. synthesized crosslinked polymers. P.B.S. and M.J.E. conducted thermal analyses. P.B.S. and R.C.B. performed dynamic mechanical analysis experiments. S.K. and C.C. performed pycnometry and thermal expansion measurements. P.B.S. and M.R.G. wrote the manuscript. All authors discussed and edited the manuscript.

Acknowledgements:
This material is based upon work supported by the U.S. Army Research Office under Grant Number W911NF-23-1-0106, the donors of the American Chemical Society Petroleum Research Fund (#62163-DNI7), and generous start-up funds from the University of Washington. M.J.E. acknowledges the National Science Foundation Graduate Research Fellowship Program (DGE-2140004) for a graduate research fellowship. DSC and DMA instrumentation were made possible through funding from the Student Technology Fund (STF) at the University of Washington. NMR spectroscopy resources at the University of Washington are supported under NIH S10 OD030224-01A1. The authors thank Prof. Dianne Xiao for use of a TGA instrument and Dr. Martin Sadilek for assistance with mass spectrometry. Prof. Aniruddh Vashisth and Dr. Naroa Sadaba are acknowledged for helpful discussions.

References:

(1) Doering, W. von E., W.; Roth, W. R. A Rapidly Reversible Degenerate Cope Rearrangement: Bicyclo[5.1.0]Octa-2,5-Diene. *Tetrahedron* **1963**, *19* (5), 715–737. https://doi.org/10.1016/S0040-4020(01)99207-5.

(2) Schröder, G. Preparation and Properties of Tricyclo[3,3,2,04,6]Deca-2,7,9-Triene (Bullvalene). *Angew. Chem. Int. Ed.* **1963**, *2* (8), 481–482. https://doi.org/10.1002/anie.196304814.

(3) Cope, A. C.; Hardy, E. M. The Introduction of Substituted Vinyl Groups. V. A Rearrangement Involving the Migration of an Allyl Group in a Three-Carbon System1. *J. Am. Chem. Soc.* **1940**, *62* (2), 441–444. https://doi.org/10.1021/ja01859a055.

(4) Bismillah, A. N.; Chapin, B. M.; Hussein, B. A.; McGonigal, P. R. Shapeshifting Molecules: The Story so Far and the Shape of Things to Come. *Chem. Sci.* **2020**, *11* (2), 324–332. https://doi.org/10.1039/C9SC05482K.

(5) Ferrer, S.; Echavarren, A. M. Synthesis of Bullvalenes: Classical Approaches and Recent Developments. *Synthesis* **2019**, *51* (5), 1037–1048. https://doi.org/10.1055/s-0037-1611637.

(6) Birvé, A. P.; Patel, H. D.; Price, J. R.; Bloch, W. M.; Fallon, T. Guest-Dependent Isomer Convergence of a Permanently Fluxional Coordination Cage. *Angew. Chem. Int. Ed.* **2022**, *61* (9), e202115468. https://doi.org/10.1002/anie.202115468.

(7) Bismillah, A. N.; Sturala, J.; Chapin, B. M.; Yufit, D. S.; Hodgkinson, P.; McGonigal, P. R. Shape-Selective Crystallisation of Fluxional Carbon Cages. *Chem. Sci.* **2018**, *9* (46), 8631–8636. https://doi.org/10.1039/C8SC04303E.

(8) Dohmen, C.; Paululat, T.; Ihmels, H. Reversible Restrain and Release of the Dynamic Valence Isomerization in a Shape-Shifting Bullvalene by Complex Formation. *Chem. – Eur. J.* **2024**, e202304311. https://doi.org/10.1002/chem.202304311.

(9) Schröder, G.; Witt, W. Crown Ethers with Fluctuating Ring Size ("Breathing Crown Ethers"). *Angew. Chem. Int. Ed.* **1979**, *18* (4), 311–312. https://doi.org/10.1002/anie.197903111.

(10) Teichert, J. F.; Mazunin, D.; Bode, J. W. Chemical Sensing of Polyols with Shapeshifting Boronic Acids As a Self-Contained Sensor Array. *J. Am. Chem. Soc.* **2013**, *135* (30), 11314–11321. https://doi.org/10.1021/ja404981q.

(11) Ferrer, S.; Echavarren, A. M. Synthesis of Barbaralones and Bullvalenes Made Easy by Gold Catalysis. *Angew. Chem. Int. Ed.* **2016**, *55* (37), 11178–11182. https://doi.org/10.1002/anie.201606101.

(12) Yahiaoui, O.; Pašteka, L. F.; Judeel, B.; Fallon, T. Synthesis and Analysis of Substituted Bullvalenes. *Angew. Chem. Int. Ed.* **2018**, *57* (10), 2570–2574. https://doi.org/10.1002/anie.201712157.

(13) Patel, H. D.; Tran, T.-H.; Sumby, C. J.; Pašteka, L. F.; Fallon, T. Boronate Ester Bullvalenes. *J. Am. Chem. Soc.* **2020**, *142* (8), 3680–3685. https://doi.org/10.1021/jacs.9b12930.

(14) Müller, A.; Haeberlen, U.; Zimmermann, H.; Poupko, R.; Luz, Z. The Pathways of the Combined Cope Rearrangement — Molecular Reorientation Process in Solid Bullvalene: A Deuterium 2D Exchange NMR Study on a Single Crystal. *Molecular Physics* **1994**, *81* (5), 1239–1258. https://doi.org/10.1080/00268979400100831.

(15) Meier, B. H.; Earl, W. L. Fluxional Behavior in the Solid State: Bullvalene. *J. Am. Chem. Soc.* **1985**, *107* (19), 5553–5555. https://doi.org/10.1021/ja00305a054.

(16) Reimers, J. R.; Li, T.; Birvé, A. P.; Yang, L.; Aragonès, A. C.; Fallon, T.; Kosov, D. S.; Darwish, N. Controlling Piezoresistance in Single Molecules through the Isomerisation of Bullvalenes. *Nat. Commun.* **2023**, *14* (1), 6089. https://doi.org/10.1038/s41467-023-41674-z.

(17) Pomfret, M. N.; Sun, P. B.; Huang, Z.; Freund, A. C.; Miyoshi, T.; Golder, M. R. Stochastic Bullvalene Architecture Modulates Structural Rigidity in π-Rich Macromolecules. *Angew. Chem. Int. Ed.* **2023**, *62* (19), e202301695. https://doi.org/10.1002/anie.202301695

(18) Willis-Fox, N.; Rognin, E.; Aljohani, T. A.; Daly, R. Polymer Mechanochemistry: Manufacturing Is Now a Force to Be Reckoned With. *Chem* **2018**, *4* (11), 2499–2537. https://doi.org/10.1016/j.chempr.2018.08.001.

(19) Ghanem, M. A.; Basu, A.; Behrou, R.; Boechler, N.; Boydston, A. J.; Craig, S. L.; Lin, Y.; Lynde, B. E.; Nelson, A.; Shen, H.; Storti, D. W. The Role of Polymer Mechanochemistry in Responsive Materials and Additive Manufacturing. *Nat. Rev. Mater.* **2021**, *6* (1), 84–98. https://doi.org/10.1038/s41578-020-00249-w.

(20) Wang, Z.; Zheng, X.; Ouchi, T.; Kouznetsova, T. B.; Beech, H. K.; Av-Ron, S.; Matsuda, T.; Bowser, B. H.; Wang, S.; Johnson, J. A.; Kalow, J. A.; Olsen, B. D.; Gong, J. P.; Rubinstein, M.; Craig, S. L. Toughening Hydrogels through Force-Triggered Chemical Reactions That Lengthen Polymer Strands. *Science* **2021**, *374* (6564), 193–196. https://doi.org/10.1126/science.abg2689.

(21) Larsen, M. B.; Boydston, A. J. "Flex-Activated" Mechanophores: Using Polymer Mechanochemistry To Direct Bond Bending Activation. *J. Am. Chem. Soc.* **2013**, *135* (22), 8189–8192. https://doi.org/10.1021/ja403757p.

(22) Zeng, T.; Ordner, L. A.; Liu, P.; Robb, M. J. Multimechanophore Polymers for Mechanically Triggered Small Molecule Release with Ultrahigh Payload Capacity. *J. Am. Chem. Soc.* **2024**, *146* (1), 95–100. https://doi.org/10.1021/jacs.3c11927.

(23) Küng, R.; Göstl, R.; Schmidt, B. M. Release of Molecular Cargo from Polymer Systems by Mechanochemistry. *Chem. – Eur. J.* **2022**, *28* (17), e202103860. https://doi.org/10.1002/chem.202103860.

(24) Davis, D. A.; Hamilton, A.; Yang, J.; Cremar, L. D.; Van Gough, D.; Potisek, S. L.; Ong, M. T.; Braun, P. V.; Martínez, T. J.; White, S. R.; Moore, J. S.; Sottos, N. R. Force-Induced Activation of Covalent Bonds in Mechanoresponsive Polymeric Materials. *Nature* **2009**, *459* (7243), 68–72. https://doi.org/10.1038/nature07970.

(25) Ducrot, E.; Chen, Y.; Bulters, M.; Sijbesma, R. P.; Creton, C. Toughening Elastomers with Sacrificial Bonds and Watching Them Break. *Science* **2014**, *344* (6180), 186–189. https://doi.org/10.1126/science.1248494.

(26) Sagara, Y.; Traeger, H.; Li, J.; Okado, Y.; Schrettl, S.; Tamaoki, N.; Weder, C. Mechanically Responsive Luminescent Polymers Based on Supramolecular Cyclophane Mechanophores. *J. Am. Chem. Soc.* **2021**, *143* (14), 5519–5525. https://doi.org/10.1021/jacs.1c01328.

(27) Wang, S.; Hu, Y.; Kouznetsova, T. B.; Sapir, L.; Chen, D.; Herzog-Arbeitman, A.; Johnson, J. A.; Rubinstein, M.; Craig, S. L. Facile Mechanochemical Cycloreversion of Polymer Cross-Linkers Enhances Tear Resistance. *Science* **2023**, *380* (6651), 1248–1252. https://doi.org/10.1126/science.adg3229.

(28) Smith, P. T.; Narupai, B.; Tsui, J. H.; Millik, S. C.; Shafranek, R. T.; Kim, D.-H.; Nelson, A. Additive Manufacturing of Bovine Serum Albumin-Based Hydrogels and Bioplastics. *Biomacromolecules* **2020**, *21* (2), 484–492. https://doi.org/10.1021/acs.biomac.9b01236.

(29) K. Andrew Miller; Dodo, O. J.; Devkota, G. P.; Kirinda, V. C.; Bradford, K. G. E.; Sparks, J. L.; Hartley, C. S.; Konkolewicz, D. Aromatic Foldamers as Molecular Springs in Network Polymers. *Chem. Commun.* **2022**, *58* (37), 5590–5593. https://doi.org/10.1039/D2CC01223E.

(30) Traeger, H.; Sagara, Y.; Berrocal, J. A.; Schrettl, S.; Weder, C. Strain-Correlated Mechanochromism in Different Polyurethanes Featuring a Supramolecular Mechanophore. *Polym. Chem.* **2022**, *13* (19), 2860–2869. https://doi.org/10.1039/D2PY00218C.

(31) Liu, C.; Morimoto, N.; Jiang, L.; Kawahara, S.; Noritomi, T.; Yokoyama, H.; Mayumi, K.; Ito, K. Tough Hydrogels with Rapid Self-Reinforcement. *Science* **2021**, *372* (6546), 1078–1081. https://doi.org/10.1126/science.aaz6694.

(32) Ito, K. Novel Cross-Linking Concept of Polymer Network: Synthesis, Structure, and Properties of Slide-Ring Gels with Freely Movable Junctions. *Polym. J.* **2007**, *39* (6), 489–499. https://doi.org/10.1295/polymj.PJ2006239.

(33) Zhao, J.; Zhang, Z.; Cheng, L.; Bai, R.; Zhao, D.; Wang, Y.; Yu, W.; Yan, X. Mechanically Interlocked Vitrimers. *J. Am. Chem. Soc.* **2022**, *144* (2), 872–882. https://doi.org/10.1021/jacs.1c10427.

(34) Hart, L. F.; Lenart, W. R.; Hertzog, J. E.; Oh, J.; Turner, W. R.; Dennis, J. M.; Rowan, S. J. Doubly Threaded Slide-Ring Polycatenane Networks. *J. Am. Chem. Soc.* **2023**, *145* (22), 12315–12323. https://doi.org/10.1021/jacs.3c02837.

(35) Yang, X.; Cheng, L.; Zhang, Z.; Zhao, J.; Bai, R.; Guo, Z.; Yu, W.; Yan, X. Amplification of Integrated Microscopic Motions of High-Density [2]Rotaxanes in Mechanically Interlocked Networks. *Nat. Commun.* **2022**, *13* (1), 6654. https://doi.org/10.1038/s41467-022-34286-6.

(36) Chen, L.; You, W.; Wang, J.; Yang, X.; Xiao, D.; Zhu, H.; Zhang, Y.; Li, G.; Yu, W.; Sessler, J. L.; Huang, F. Enhancing the Toughness and Strength of Polymers Using Mechanically Interlocked Hydrogen Bonds. *J. Am. Chem. Soc.* **2024**, *146* (1), 1109–1121. https://doi.org/10.1021/jacs.3c12404.

(37) Song, Y.; Liu, Y.; Qi, T.; Li, G. L. Towards Dynamic but Supertough Healable Polymers through Biomimetic Hierarchical Hydrogen-Bonding Interactions. *Angew. Chem. Int. Ed.* **2018**, *57* (42), 13838–13842. https://doi.org/10.1002/anie.201807622.

(38) Xing, P.; Li, Y.; Xue, S.; Fiona Phua, S. Z.; Ding, C.; Chen, H.; Zhao, Y. Occurrence of Chiral Nanostructures Induced by Multiple Hydrogen Bonds. *J. Am. Chem. Soc.* **2019**, *141* (25), 9946–9954. https://doi.org/10.1021/jacs.9b03502.

(39) Zhang, Q.; Li, T.; Duan, A.; Dong, S.; Zhao, W.; Stang, P. J. Formation of a Supramolecular Polymeric Adhesive via Water–Participant Hydrogen Bond Formation. *J. Am. Chem. Soc.* **2019**, *141* (20), 8058–8063. https://doi.org/10.1021/jacs.9b02677.

(40) Diao, K.; J. Whitaker, D.; Huang, Z.; Qian, H.; Ren, D.; Zhang, L.; Li, Z.-Y.; Sun, X.-Q.; Xiao, T.; Wang, L. An Ultralow-Acceptor-Content Supramolecular Light-Harvesting System for White-Light Emission. *Chem. Commun.* **2022**, *58* (14), 2343–2346. https://doi.org/10.1039/D1CC06647A.

(41) Zhukhovitskiy, A. V.; Zhong, M.; Keeler, E. G.; Michaelis, V. K.; Sun, J. E. P.; Hore, M. J. A.; Pochan, D. J.; Griffin, R. G.; Willard, A. P.; Johnson, J. A. Highly Branched and Loop-Rich Gels via Formation of Metal–Organic Cages Linked by Polymers. *Nat. Chem.* **2016**, *8* (1), 33–41. https://doi.org/10.1038/nchem.2390.

(42) McConnell, A. J.; Wood, C. S.; Neelakandan, P. P.; Nitschke, J. R. Stimuli-Responsive Metal–Ligand Assemblies. *Chem. Rev.* **2015**, *115* (15), 7729–7793. https://doi.org/10.1021/cr500632f.

(43) Yount, W. C.; Loveless, D. M.; Craig, S. L. Small-Molecule Dynamics and Mechanisms Underlying the Macroscopic Mechanical Properties of Coordinatively Cross-Linked Polymer Networks. *J. Am. Chem. Soc.* **2005**, *127* (41), 14488–14496. https://doi.org/10.1021/ja054298a.

(44) Beck, J. B.; Rowan, S. J. Multistimuli, Multiresponsive Metallo-Supramolecular Polymers. *J. Am. Chem. Soc.* **2003**, *125* (46), 13922–13923. https://doi.org/10.1021/ja038521k.

(45) Hailes, R. L. N.; Oliver, A. M.; Gwyther, J.; Whittell, G. R.; Manners, I. Polyferrocenylsilanes: Synthesis, Properties, and Applications. *Chem. Soc. Rev.* **2016**, *45* (19), 5358–5407. https://doi.org/10.1039/C6CS00155F.

(46) Jones, B. H.; Wheeler, D. R.; Black, H. T.; Stavig, M. E.; Sawyer, P. S.; Giron, N. H.; Celina, M. C.; Lambert, T. N.; Alam, T. M. Stress Relaxation in Epoxy Thermosets via a Ferrocene-Based Amine Curing Agent. *Macromolecules* **2017**, *50* (13), 5014–5024. https://doi.org/10.1021/acs.macromol.7b00501.

(47) Achard, M.; Mosrin, M.; Tenaglia, A.; Buono, G. Cobalt(I)-Catalyzed [6+2] Cycloadditions of Cyclooctatetra(Tri)Ene with Alkynes. *J. Org. Chem.* **2006**, *71* (7), 2907–2910. https://doi.org/10.1021/jo052630v.

(48) Zimmerman, H. E.; Mariano, P. S. Mechanistic and Exploratory Organic Photochemistry. XLI. Di-.Pi.-Methane Rearrangement. Interaction of Electronically Excited Vinyl Chromophores. *J. Am. Chem. Soc.* **1969**, *91* (7), 1718–1727. https://doi.org/10.1021/ja01035a021.

(49) Zimmerman, H. E.; Grunewald, G. L. The Chemistry of Barrelene. III. A Unique Photoisomerization to Semibullvalene. *J. Am. Chem. Soc.* **1966**, *88* (1), 183–184. https://doi.org/10.1021/ja00953a045.

(50) Zimmerman, H. E.; Binkley, R. W.; Givens, R. S.; Sherwin, M. A. Mechanistic Organic Photochemistry. XXIV. The Mechanism of the Conversion of Barrelene to Semibullvalene. A General Photochemical Process. *J. Am. Chem. Soc.* **1967**, *89* (15), 3932–3933. https://doi.org/10.1021/ja00991a064.

(51) Heimenz, P. C.; Lodge T. P. *Polymer Chemistry*; CRC Press, 2007

(52) Li, G.; Lee-Sullivan, P.; Thring, R. W. Determination of Activation Energy for Glass Transition of an Epoxy Adhesive Using Dynamic Mechanical Analysis. *Journal of Thermal Analysis and Calorimetry* **2000**, *60* (2), 377–390. https://doi.org/10.1023/A:1010120921582.

(53) Haward, R. N.; Young, R. J. *The Physics of Glassy Polymers*; Chapman & Hall, 1997

(54) Kausch, H. H.; Hassel, J. A.; Jaffee, R. I. *Deformation and Fracture of High Polymers*; Plenum Press, 1973